Energy Advances

ROYAL SOCIETY OF CHEMISTRY

PAPER

View Article Online
View Journal | View Issue

Cite this: *Energy Adv.*, 2023, 2, 1036

Ultra-low cost supercapacitors from coal char: effect of electrolyte on double layer capacitance†

Zahra Karimi,[a] Jaron Moon,[a] Joshua Malzahn,[b] Eric Eddings[b] and Roseanne Warren *[a]

Received 7th February 2023,
Accepted 15th May 2023

DOI: 10.1039/d3ya00064h

rsc.li/energy-advances

Electrochemical double-layer capacitors (EDLCs) provide high power density and long cycle life energy storage. This work examines the use of inexpensive, raw coal char as an electrode material for supercapacitors. The effect of electrolyte composition on the performance of coal char supercapacitors is explored for the first time to determine the relative contributions of double-layer capacitance *vs.* faradaic reactions on total charge storage. Six electrolytes are examined with coal char electrodes, including: four aqueous electrolytes (0.5 M H_2SO_4, 6 M KOH, 0.5 M Na_2SO_4, 4 M $LiNO_3$); a water-in-salt electrolyte using 13 m $NaClO_4$; and an ionic liquid electrolyte (1-butyl-3-methylimidazolium tetrafluoroborate in acetonitrile). Voltage range, specific capacitance, electrochemical impedance, and charge–discharge characteristics of the coal char in the different electrolytes are characterized. The results indicate that neutral aqueous, water-in-salt, and ionic liquid electrolytes present a charging/discharging process approaching ideal EDLC behavior. The study provides insight into the optimal electrolyte composition for use with coal char electrodes and contributes to the current understanding of electrode-electrolyte interactions in carbon supercapacitors.

1. Introduction

Supercapacitors are electrochemical energy storage devices bridging the gap between batteries and capacitors. Supercapacitors are characterized by high specific power density, high charge–discharge rates, and long cycle life typically exceeding one million cycles.[1] Despite these advantages, the high cost and low energy density of supercapacitors currently restrict their applications to those demanding high power delivery in a short time.[2] Supercapacitor electrode materials are classified as electrochemical double-layer capacitors (EDLCs) or pseudocapacitors.[3,4] EDLCs store energy electrostatically *via* charge separation at the electrode-electrolyte interface, while pseudocapacitors employ: reversible surface redox reactions, underpotential deposition, and/or electrosorption mechanisms of charge storage.[5]

A wide variety of carbon materials have been explored as electrode materials in EDLCs. High cost and complex synthesis procedures, however, limit the widespread use of many carbon materials in EDLCs.[3] Among carbon materials, those with low cost, high abundance, and eco-friendly character are of particular interest. Increasing the voltage range of EDLCs through careful selection of electrode-electrolyte combinations is an effective strategy for improving energy density, as capacitive energy density is proportional to cell voltage squared. The choice of electrolyte ion and solvent is an important consideration affecting electrolyte conductance, ion adsorption, and electrolyte dielectric properties, all of which determine cell equivalent series resistance and specific capacitance.[6] The voltage window of an electrolyte is governed by the electrochemical stability of both the solvent and the ionic species.[6]

Coal is a cheap and abundant carbon-rich material. When coal is heated in an inert atmosphere, it decomposes into volatiles, tar, and char. Char is the major constituent, comprising upwards of 20–85% by mass of many coals.[7] Char consists of hard carbons, high molecular weight hydrocarbons, and ash. As coal-based power generation is reduced worldwide, alternative uses of coal constituents are being pursued. Coal ash is a valuable source of rare earth elements.[8] Tar can be processed into high-value carbon products including graphene[9] and carbon fiber.[10] Coal char, however, is largely a waste material. This work contributes to current research efforts in the fossil energy sector by exploring a potential high-value application of untreated coal char as an electrochemical double layer capacitor. Given the ultra-low cost of untreated char (US$ 0.11 per kg)[11] compared to activated carbons (US$ 2.8 per kg),[12] the application of raw char as a supercapacitor material is worth evaluating.

[a] *Department of Mechanical Engineering, University of Utah 1495 E 100 S, Salt Lake City 1550 MEK, Utah, 84112, USA. E-mail: roseanne.warren@utah.edu*
[b] *Department of Chemical Engineering, University of Utah 50 S. Central Campus Dr, Salt Lake City 3290 MEB, UT 84112, USA*

† Electronic supplementary information (ESI) available. See DOI: https://doi.org/10.1039/d3ya00064h

Prior reports of coal char-based supercapacitors typically perform extensive chemical and physical treatments on the char prior to use as a supercapacitor electrode.[13–15] Yaglicki *et al.* selected high-sulfur coal char as a supercapacitor precursor to eliminate a S doping step, however their chemical activation process still included high concentration HCl and HF washing.[13] The authors noted that these treatments significantly increase process complexity and cost. Other studies on coal char-derived supercapacitor electrodes have employed: HCl washing;[14] ultrasonic-assisted chemical activation;[15] NH_4Cl-assisted KOH-activation, with HCl and HF washing;[16] and physical activation with CO_2 and H_2O.[17] To date, there have been no investigations of untreated coal char as a supercapacitor electrode material. Additionally, there have been no studies examining the effect of electrolyte composition on non-activated coal char supercapacitors.

This work investigates bituminous-grade coal char from a Utah mine as an ultra-low-cost carbon material for supercapacitor electrodes. The char is untreated except for a preliminary pyrolysis step to remove volatiles. Six electrolytes are tested with the coal char electrodes: four aqueous solutions (0.5 M H_2SO_4, 6 M KOH, 0.5 M Na_2SO_4, and 4 M $LiNO_3$); a water-in-salt (WIS) electrolyte using 13 m $NaClO_4$; and 1-butyl-3-methylimidazolium tetrafluoroborate ionic liquid (IL) in acetonitrile (BMIM BF_4/AN). While pure carbon electrodes may be expected to exhibit ideal double-layer capacitance within the electrochemically stable voltage window of an electrolyte, the behavior to chemically complex, carbon-based materials like untreated coal char in a given electrolyte is not known *a priori.* In this work, untreated coal char electrodes are tested over their expected voltage windows in each electrolyte, and the range over which the char exhibits pure double layer capacitance is identified. The results provide insights into the optimal electrolyte composition and suitable operative windows for use with untreated coal char supercapacitor electrodes.

2. Experimental

2.1 Materials

Raw bituminous coal powder was obtained from the Sufco mine (Sevier County, Utah). All other chemicals were obtained from Millipore Sigma.

2.2 Coal char preparation and characterization

Ultimate analysis and ash elemental analysis of Sufco coal was done pre-pyrolyzation. Pulverized coal was pyrolyzed at 900 °C in a fixed bed reactor under N_2 atmosphere. The coal was heated to 900 °C in 1 hour, followed by 20 min at temperature, then passively cooled to room temperature under N_2 atmosphere. The pyrolyzed coal char was characterized *via* scanning electron microscope (SEM) imaging and K-alpha energy-dispersive X-ray spectroscopy (EDS) using an FEI Quanta 600F SEM. EDS results were collected from three different points on the surface of the sample and the mean value reported.

Pore size distribution and specific surface area of the coal char post-pyrolysis were determined from N_2 and CO_2 adsorption measurements performed by Anton Paar using an Autosorb®-iQ. Samples were outgassed at 300 °C for 12 hours before measurement. To determine the surface area and pore size distribution from CO_2 measurements, adsorption/desorption isotherms were fitted with data collected from several grand canonical Monte Carlo (GCMC) kernels calculated on carbons with different pore sizes. Specific surface area was determined from N_2 adsorption/desorption isotherms using the Brunauer–Emmett–Teller (BET) method. A Monte Carlo method was used to determine pore size distribution from the N_2 adsorption/desorption isotherms.

X-ray photoelectron spectroscopy (XPS) was conducted using a Kratos Axis Ultra instrument with monochromatic Al Kα source. C 1s peak of adventitious carbon was used as an internal standard to correct the binding energy on narrow scan spectra.

2.3 Supercapacitor electrode preparation

Pyrolyzed coal char was milled using an electric grinder and sieved to a particle size $\leq$ 53 μm. Supercapacitor electrodes were prepared using a mixture of 80 wt% coal char, 10 wt% SuperP, and 10 wt% polyvinylidene fluoride (PVDF). N,N-dimethylformamide (DMF) was used as a dispersive medium to form a homogeneous slurry. Stainless steel current collector disks (316 SS) were sanded with P220 sandpaper sheets, then cleaned with acetone before electrode coating. The prepared slurry was coated on the stainless-steel disks and baked at 65 °C for 24 h. The total mass loading of coal char, SuperP, and PVDF slurry was 7 mg cm^{-2} per electrode; electrode area was 1.89 cm^{-2}.

2.4 Electrochemical testing

Electrochemical testing was done using a Gamry Interface 1000E potentiostat. Cyclic voltammetry (CV), galvanostatic charge–discharge (GCD), and electrochemical impedance spectroscopy (EIS) measurements were conducted in a symmetric two-electrode configuration using a Conflat-type cell.[18] The following electrolytes were used: 6 M KOH, 0.5 M H_2SO_4, 0.5 M Na_2SO_4, 13 m $NaClO_4$, and 4 M $LiNO_3$ in water; and BMIM BF_4/AN (1 : 1 wt%). Electrolyte concentrations were chosen to match those frequently reported in investigations of coal char- and other carbon-based supercapacitors (Table S1, ESI†). Two 38 μm thick Celgard 2340 trilayer microporous membranes (polypropylene/polyethylene/polypropylene) were used as the separator. Electrodes and separator were immersed in electrolyte for 1 h before assembling the cells. EIS measurements were conducted from 100 mHz to 100 kHz with 10 mV alternating current amplitude. Equivalent circuit models generated using Gamry Echem Analyst™ software were used to calculate cell equivalent series resistance and charge-transfer resistance.

The specific capacitance (F g^{-1}) of coal char in each electrolyte was calculated from two-electrode CV

measurements using eqn (1):

$$C_{\text{cell, CV}} = \frac{\int_{V_1}^{V_2} I(V)\mathrm{d}V}{2 \times \Delta V \times v \times m} \quad (1)$$

where $I(V)$ is the measured current between voltages V_1 and V_2, $\int_{V_1}^{V_2} I(V)\mathrm{d}V$ is the integrated area under the CV curve, ΔV is the scanned potential window, v is the scan rate (V s^{-1}), and m is the combined mass of electrode material for both electrodes. Specific capacitance was calculated from GCD measurements using eqn (2):

$$C_{\text{cell, GCD}} = \frac{I \times \Delta t}{m \times \Delta V} \quad (2)$$

where I is the discharge current, Δt is the discharge time interval for a voltage range ΔV, and m is the combined mass of electrode material for both electrodes. Energy density (Wh kg^{-1}) and power density (W kg^{-1}) were calculated using eqn (3) and (4), respectively:

$$E = \frac{C_{\text{cell,GCD}} \times \Delta V^2}{2} \quad (3)$$

$$P = \frac{E}{\Delta t} \quad (4)$$

3. Results and discussion

3.1. Coal char characterization

Ultimate analysis of the pre-pyrolyzed coal char indicates that Sufco coal is low-sulfur coal and contains approximately 13% ash by weight (Table S2, ESI†). The ash is primarily composed of silicon, calcium, aluminum, sulfur, titanium, and iron oxides (Table S3, ESI†). Fig. 1 provides SEM images of coal char post-pyrolyzation. The char has a non-uniform surface morphology with a dense structure and no visible pores. Homogeneously distributed small crystallites (*i.e.* minerals) and large layers of carbon sheets are observed on the surface of the char particles. EDS measurements indicate that the major elements of the coal char post-pyrolysis are C, O, Si, and Ca (Table S4, ESI†).

Fig. 2 compares pore size distributions of the coal char calculated from N_2 (Fig. 2a) and CO_2 (Fig. 2b) adsorption measurements. The N_2 isotherm shows low N_2 uptake and pronounced hysteresis (Fig. S1a, ESI†). The specific surface area of the coal char post-pyrolysis calculated from the N_2 isotherms is 17.791 m^2 g^{-1}. The N_2 pore size distribution (Fig. 2a) indicates a significant concentration of 15 Å wide pores. CO_2 adsorption/desorption isotherms at 0 °C provide a better measurement of coal char microporosity and specific surface area due to the smaller kinetic diameter of CO_2 and the higher analysis temperature (Fig. S1b and c, ESI†). The specific surface area of the coal char calculated from the CO_2 isotherm is 372.567 m^2 g^{-1}, and the total pore volume is 0.100 cm^3 g^{-1}. The pore size distribution (Fig. 2b) indicates high microporosity with significant concentrations of 5 Å and 6 Å wide pores.

XPS was used to detect the surface chemical composition of the coal char (Fig. 3). The broad spectrum shows six species: C, O, Si, Ca, Al and F (Fig. 3a). The shape of the C KLL Auger spectrum of carbon indicates sp^2 (graphite) and sp^3 (diamond) hybridization. D parameter, the energy difference between the maximum and minimum of the first derivative of C KLL spectrum, determines the C sp^2/sp^3 content. According to Lascovich and Scaglione,[19] D values for diamond and graphite samples are 14.3 and 22.5 respectively. The D parameter for the coal char sample is 17, which indicates a graphite-like structure with high C sp^2 content. The C1s narrow scan of the coal char can be fitted with: C sp^2 (~284.5 eV), C sp^3 (~285.4 eV), C–O (~286.1 eV), C═O (~287.0 eV), C(O)–OH (~288.4 eV), O–C(O)–O (~289.6 eV), and C–F_2 (~290.9 eV) (Fig. 3b).[20] The O1s narrow scan for coal char was fitted with: Al_2O_3 (~530.5 eV),[21] CaO (~531.5 eV),[21] O═C (~531.6 eV),[22] O–C (~532.2 eV),[23] O-Si (~533.6 eV),[24] and surface adsorbed H_2O (~535 eV)[22] (Fig. 3c). The high O content of the untreated coal char is likely to increase hydrophilicity of coal char supercapacitor electrodes compared to low O carbons.[5,25] The presence of O═C functional groups is a cause of high pseudocapacitance in untreated coal char electrodes. While this will lead to increased overall specific capacitance, the potential for higher self-discharge should be noted.[5]

3.2. Cyclic voltammetry

CV measurements of two-electrode symmetrical supercapacitor cells were conducted to determine the voltage window of the coal char in various electrolytes (Fig. 4). The quasi-rectangular

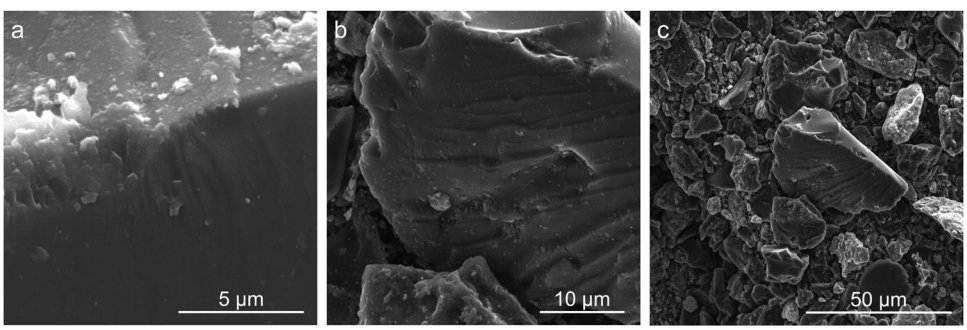

Fig. 1 SEM images of Sufco coal char particles post-pyrolysis.

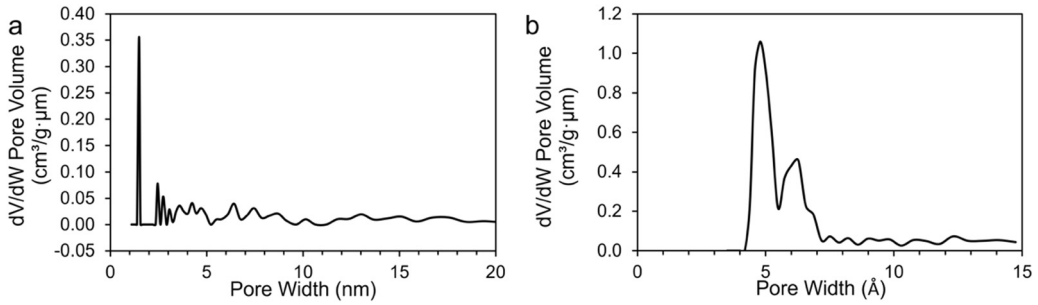

Fig. 2 Pore size distribution of coal char post-pyrolysis calculated from (a) N_2 and (b) CO_2 adsorption measurements.

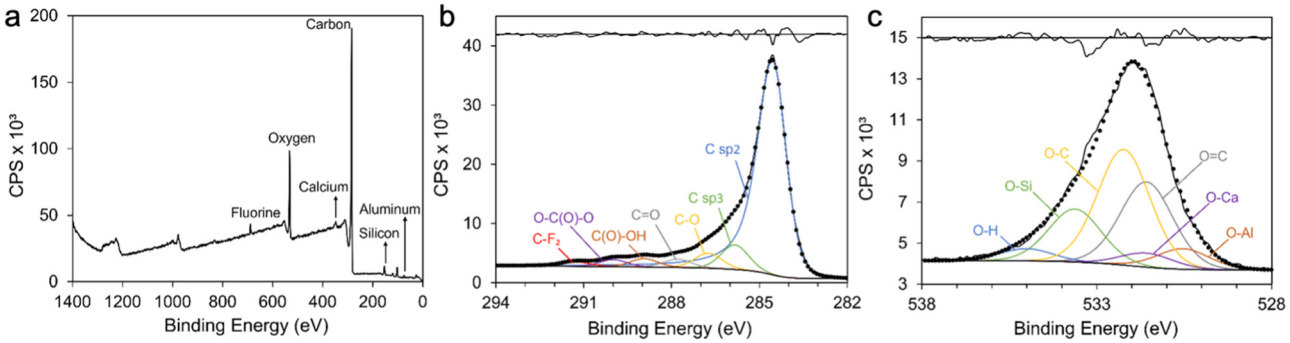

Fig. 3 XPS spectra of coal char including: (a) survey spectra; (b) C1s and (c) O1s narrow scans. Residual standard deviations of peak fittings are provided in (b) and (c) (upper black lines).

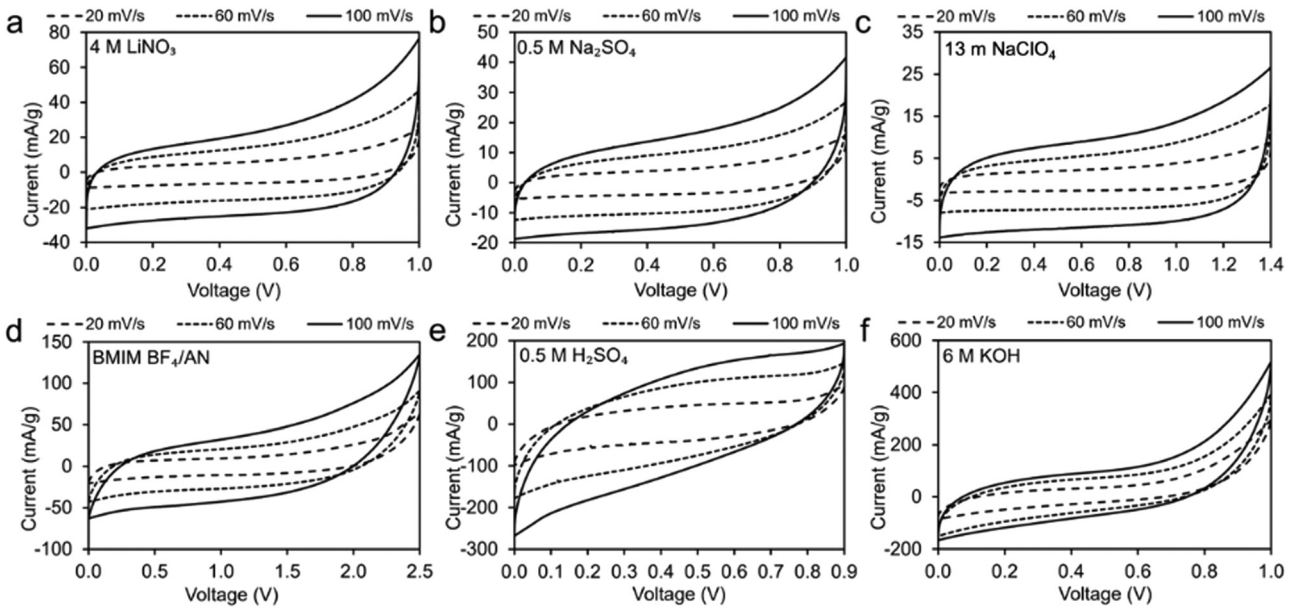

Fig. 4 CV measurements of coal char electrodes in: (a) 4 M $LiNO_3$, (b) 0.5 M Na_2SO_4, (c) 13 m $NaClO_4$, (d) BMIM BF_4/AN, (e) 0.5 M H_2SO_4 and (f) 6 M KOH at scan rates of 20, 60, and 100 mV s^{-1}.

shapes of the CV plots indicate varying degrees of ideal EDLC behavior. The observed 1.0 V voltage window for neutral (0.5 M Na_2SO_4, 4 M $LiNO_3$) and basic (6 M KOH) electrolytes is consistent with expectations for EDLCs in aqueous electrolytes. Voltage windows for 13 m $NaClO_4$ (1.4 V) and BMIM BF_4/AN (2.5 V) electrolytes are less than other reported carbon

supercapacitor voltage windows for these electrolytes. This may be due to impurities in the coal char limiting EDLC range. Neutral aqueous, WIS, and IL electrolytes present CV curves most similar to those of ideal EDLCs (Fig. 4a–d). More significant deviations from ideal are observed for strongly acidic (Fig. 4e) and strongly basic electrolytes (Fig. 4f).

Fig. 5a plots CV curves for each electrolyte at 100 mV s^{-1} on a common scale. The higher specific capacitance observed for 6 M KOH and 0.5 M H_2SO_4 electrolytes (1.5 F g^{-1} and 1.7 F g^{-1}, respectively, at 20 mV s^{-1}) can be attributed to higher CV currents compared to the other electrolytes. Coal char in BMIM BF_4/AN IL achieves the third-highest specific capacitance (1.03 F g^{-1} at 20 mV s^{-1}) by virtue of a large voltage window. With increasing scan rate, specific capacitance decreases most significantly for 6 M KOH and 0.5 M H_2SO_4 electrolytes (Fig. 5b). Change in capacitance with repeated cycling was investigated for each electrolyte over 100 cycles at a scan rate of 100 mV s^{-1} (Fig. 5c). Cells with BMIM BF_4/AN, 13 m $NaClO_4$, and 0.5 M Na_2SO_4 electrolytes exhibit some initial capacity fade relative to cycle 3, retaining 90% of their capacitance after 100 cycles. Cells with 4 M $LiNO_3$ and 6 M KOH electrolytes show a minor change in capacity over 100 cycles (<3%). With 0.5 M H_2SO_4 electrolyte, capacity increased 12% after 100 cycles compared to the third discharge cycle. This may be due to increasing char porosity and/or pore accessibility arising from ash removal. H_2SO_4 is commonly used for deashing coal char.[26]

To quantify double layer *vs.* faradaic contributions to specific capacitance, current response at a fixed potential can be separated into non-faradaic surface capacitive ($k_1\nu$) and faradaic charge transport processes ($k_2\nu^{1/2}$) according to the current partitioning equation (eqn (5)):[27]

$$I(V)/\nu^{1/2} = k_1\nu^{1/2} + k_2 \quad (5)$$

Fig. S2 (ESI†) plots eqn (5) for all electrolytes at varying cell voltages.

Fig. 6a–f compares total and capacitive current responses at 100 mV s^{-1} scan rate. Regions bound by capacitive current lines (shaded areas) are indicative of EDLC contributions to total capacitance. The plots enable identification of voltage ranges over which untreated coal char electrodes have nearly 100% double layer capacitance, reducing potential overcharging and subsequent self-discharge. Vertical dashed lines in each plot indicate the voltage range over which the capacitive current could be calculated, assuming capacitive current must always be less than total current. In the case of 4 M $LiNO_3$, 0.5 M Na_2SO_4, 13 m $NaClO_4$, and BMIM BF_4/AN electrolytes (Fig. 6a–d, respectively), most of the total current is non-faradaic. Proportionally lower capacitive currents are observed for 0.5 M H_2SO_4 (Fig. 6e) and 6 M KOH electrolytes (Fig. 6f). Fig. 6g compares the specific capacitance contributions of the shaded areas with the total specific capacitance of the electrodes at varying scan rates. At 100 mV s^{-1}, capacitive effects contribute 83% (13 m $NaClO_4$), 75.4% (4 M $LiNO_3$), 68.5% (0.5 M Na_2SO_4), 64% (BMIM BF_4/AN), 45% (6 M KOH), and 34% (0.5 M H_2SO_4) of total specific capacitance in each electrolyte. At slower scan rates, capacitive effects contribute proportionally less to total capacitance in all electrolytes, as slower rates enable more faradaic processes.[28] For maximum cycle life and minimum self-discharge, untreated coal char electrodes should be operated within the Fig. 6 voltage windows over which their response approaches ideal double layer capacitance in each electrolyte.

3.3. Chronopotentiometry

Fig. 7 provides GCD results for symmetric two-electrode coal char cells in the six different electrolytes. Table 1 compares specific capacitance values obtained from two-electrode CV measurements with values determined from GCD measurements. For this comparison, the discharge current was kept at 100 mA for all samples. The results show good agreement.

Table 2 compares maximum capacitance, power and energy density values for coal char with literature values reported for higher-cost carbons in the same electrolytes. The highest coal char specific capacitance values of 11.61 F g^{-1} and 10.81 F g^{-1} were achieved in 6 M KOH at 8 mA applied current (713 mA g^{-1}) and in 0.5 M H_2SO_4 at 0.6 mA applied current (44.3 mA g^{-1}), respectively. Coal char electrodes showed the highest values of energy density in 6 M KOH and 13 m $NaClO_4$ electrolytes, and the highest value of power density in 4 M $LiNO_3$. Energy densities for the raw coal char electrodes tested here are

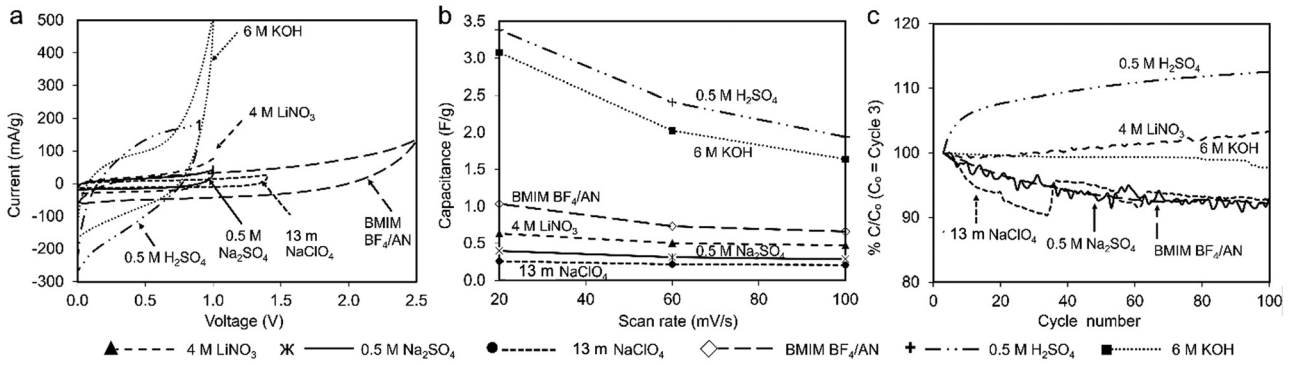

Fig. 5 (a) CV curves for all tested electrolytes (100 mV s^{-1}). (b) Specific capacitance at different scan rates for each electrolyte. (c) Capacitance retention (% of cycle 3 specific capacitance) over 100 cycles (100 mV s^{-1}).

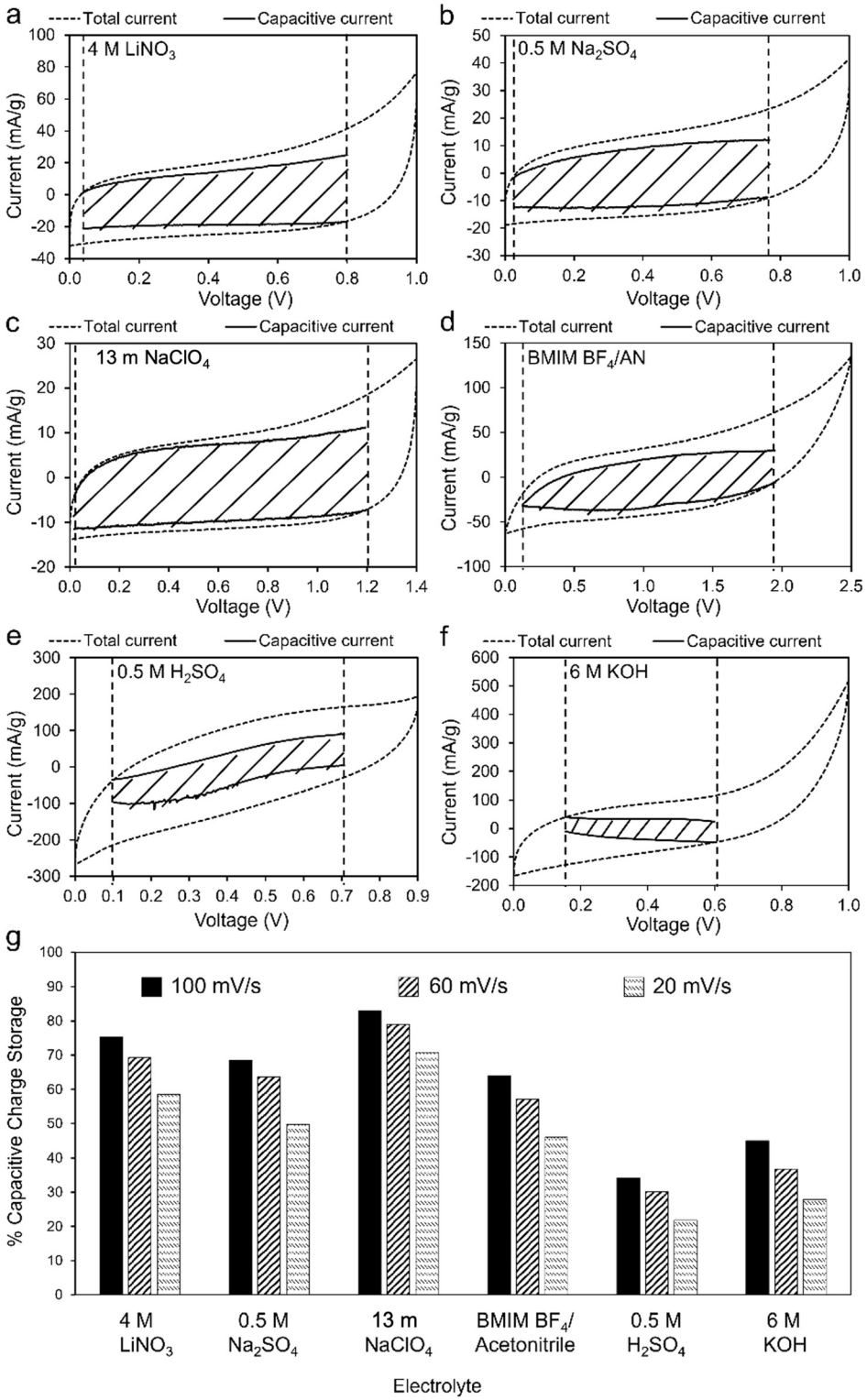

Fig. 6 (a)–(f) CV measurements (100 mV s^{-1}) of two-electrode coal char cells in: (a) 4 M $LiNO_3$, (b) 0.5 M Na_2SO_4, (c) 13 m $NaClO_4$, (d) BMIM BF_4/AN, (e) 0.5 M H_2SO_4 and (f) 6 M KOH electrolytes. Total current (dashed line) is obtained experimentally. Capacitive (*i.e.* non-faradaic) current (black solid lines bounding shaded regions) is determined from eqn (5). (g) Comparison of EDLC charge storage contributions as a % of total specific capacitance for each electrolyte at scan rates of 20, 60, and 100 mV s^{-1}.

generally lower than literature reports for higher-cost carbons, however, the ultra-low cost of coal char and the favorable comparison in some electrolytes suggests that untreated coal char would benefit from additional consideration as a supercapacitor electrode material. We note that the energy density achieved for coal char in 6 M KOH exceeds that reported for

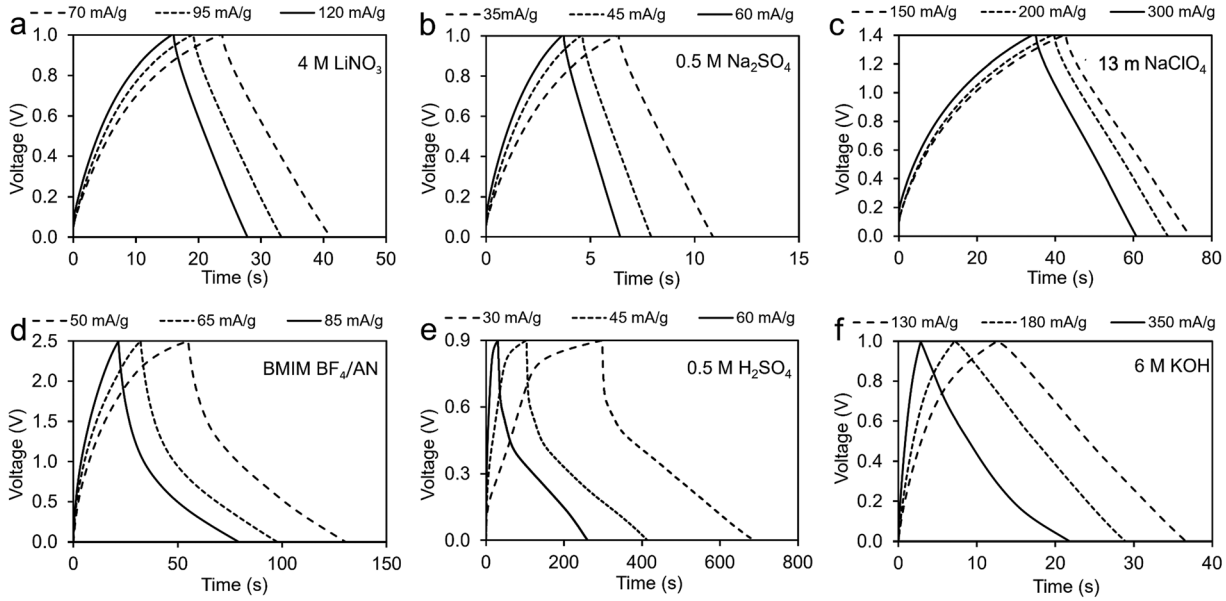

Fig. 7 GCD measurements of coal char in: (a) 4M $LiNO_3$, (b) 0.5 M Na_2SO_4, (c) 13 m $NaClO_4$, (d) BMIM BF_4/AN, (e) 0.5 M H_2SO_4, and (f) 6 M KOH electrolytes.

Table 1 Voltage window and specific capacitance of coal char in different electrolytes

			CV capacitance (F g^{-1})			
			Scan rate (mV s^{-1})			
Electrolyte		Voltage window (V)	100	60	20	GCD capacitance (F g^{-1})
WIS	13 m $NaClO_4$	1.5	0.10	0.11	0.13	0.19
Aqueous	6 M KOH	1.0	1.46	1.80	2.75	1.94
	0.5 M H_2SO_4	0.9	0.97	1.20	1.69	2.00
	4 M $LiNO_3$	1.0	0.24	0.25	0.32	0.32
	0.5 M Na_2SO_4	1.0	0.14	0.16	0.20	0.17
IL	BMIM BF_4/AN	2.5	0.33	0.37	0.52	0.43

Table 2 Discharge specific capacitance, energy density, and power density of coal char in different electrolytes

				Literature		
Electrolyte	Capacitance (F g^{-1})	Power density (W kg^{-1})	Highest energy density (Wh kg^{-1})	Energy density (Wh kg^{-1})	Electrode material	Ref.
13 m $NaClO_4$	4.31	615.28	5.76 (850 mA g^{-1})	17.5 (500 mA g^{-1})	Graphene	30
6 M KOH	11.61	478.78	5.26 (700 mA g^{-1})	4.4 (200 mA g^{-1})	Seaweed carbons	29
0.5 M H_2SO_4	10.81	37.66	2.44 (60 mA g^{-1})	12.6 (200 mA g^{-1})	Seaweed carbons	29
4 M $LiNO_3$	1.33	778.52	1.34 (600 mA g^{-1})	21.16	Porous AC	31
0.5 M Na_2SO_4	0.23	62.34	0.15 (60 mA g^{-1})	10.7 (200 mA g^{-1})	Seaweed carbons	29
BMIM BF_4/AN	1.42	140.11	2.29 (85 mA g^{-1})	29.2 (1 A g^{-1})	Graphene nanosheets	32

seaweed-derived activated carbon,[29] with the coal char electrodes tested at a higher discharge current. With 13 m $NaClO_4$, untreated coal char energy density is only 3× lower than graphene, a surprising result for such a low-cost material with minimal processing.[30]

3.4. EIS

EIS measurements were conducted on two-electrode symmetric cells (Fig. 8). The equivalent circuit model that best fits the EIS is a Randles equivalent circuit with a constant phase element (CPE). Bode plots showing goodness of fit of the equivalent circuit model are provided in Fig. S3; Table S5 and S6 (ESI†) provide equivalent circuit parameters used in the fitting models. Nyquist plots exhibit semicircular features in the high frequency regime (indicative of charge transfer resistance) and a straight line in the low frequency regime (indicative of ion diffusion). All cells have low equivalent series resistance ($R_s < 2\ \Omega$) indicating good conductivity of the electrolytes

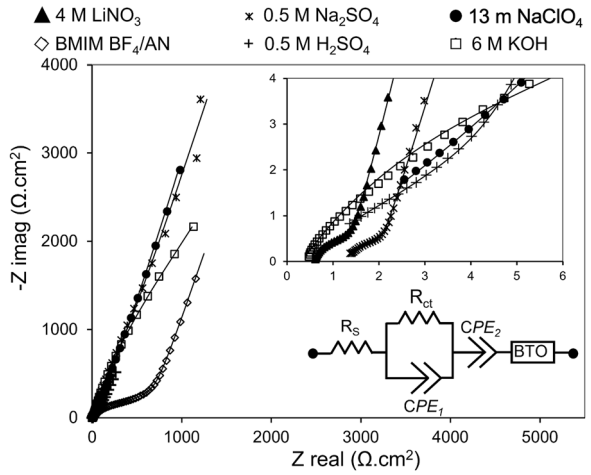

Fig. 8 EIS measurements of coal char electrodes presented as a normalized Nyquist plot. Upper inset: High-frequency behavior. Lower inset: Randles equivalent circuit model with series resistance R_s, charge transfer resistance R_{ct}, constant phase elements (CPE_1 and CPE_2), and Bisquert Open (BTO) circuit elements.

(except BMIM BF_4/AN, which has $R_s > 10$ Ω). Charge transfer resistance (R_{ct}) is lowest for 4 M $LiNO_3$, 0.5 M Na_2SO_4, and 6 M KOH electrolytes; moderately high for 0.5 M H_2SO_4 and 13 m $NaClO_4$ electrolytes; and high for BMIM BF_4/AN. R_{ct} for BMIM BF_4/AN exceeds that of the aqueous electrolytes due to the higher viscosity and lower ionic conductivity of IL electrolytes.

4. Conclusion

This work demonstrates the effects of electrolyte composition on the supercapacitor performance of untreated coal char electrodes. The results indicate that char is a promising low cost electrode material for EDLCs. Non-faradaic charge storage predominates in neutral aqueous, WIS, and IL electrolytes with a charging/discharging process approaching ideal EDLC behavior. A deviation from ideal EDLC behavior is observed for strongly acidic (0.5 M H_2SO_4) and strongly basic (6 M KOH) electrolytes leading to higher specific capacitance. The ultra-low cost of coal char and its favorable comparison with high-cost carbons in some electrolytes suggests that coal char would benefit from additional consideration as a supercapacitor material.

Author contributions

Z. Karimi: conceptualization, data curation, investigation, methodology, visualization, writing; J. Moon, J. Malzahn: investigation, methodology; E. Eddings: conceptualization, resources, validation; R. Warren: conceptualization, resources, funding acquisition, validation, writing.

Conflicts of interest

There are no conflicts of interest to declare.

Acknowledgements

This work is supported in part by NSF Award #1742696 and #2152562. The authors are grateful to Dr Matthew Linford for helpful discussions regarding XPS results.

References

1 S. Huang, X. Zhu, S. Sarkar and Y. Zhao, *APL Mater.*, 2019, **7**, 100901.
2 J. Zhao and A. F. Burke, *J. Energy Chem.*, 2021, **59**, 276–291.
3 G. Wang, L. Zhang and J. Zhang, *Chem. Soc. Rev.*, 2012, **41**, 797–828.
4 S. Zheng, Q. Li, H. Xue, H. Pang and Q. Xu, *Natl. Sci. Rev.*, 2020, **7**, 305–314.
5 B. E. Conway, V. Birss and J. Wojtowicz, *J. Power Sources*, 1997, **66**, 1–14.
6 B. E. Conway, *Electrochemical Supercapacitors: Scientific Fundamentals and Technological Applications*, Springer Science + Business Media, New York, 1999.
7 H. H. Schobert, *Coal: The Energy Source of the Past and Future*, American Chemical Society, Washington, DC, 1987.
8 V. K. Kuppusamy, A. Kumar and M. Holuszko, *J. Energy Resour. Technol.*, 2019, **141**, 070708.
9 H. Xu, Q. Lin, T. Zhou, T. Chen, S. Lin and S. Dong, *J. Anal. Appl. Pyrolysis*, 2014, **110**, 481–485.
10 C. Banerjee, V. K. Chandaliya and P. S. Dash, *J. Anal. Appl. Pyrolysis*, 2021, **158**, 105272.
11 O. Soka and O. Oyekola, *Heliyon*, 2020, **6**, e04346.
12 M. León, J. Silva, S. Carrasco and N. Barrientos, *Processes*, 2020, **8**, 945.
13 S. Yaglikci, Y. Gokce, E. Yagmur, A. Banford and Z. Aktas, *Surf. Interfaces*, 2021, **22**, 100899.
14 T. Islam, M. M. Hasan, S. S. Shah, M. R. Karim, F. S. Al-Mubaddel, M. H. Zahir, M. A. Dar, M. D. Hossain, M. A. Aziz and A. J. S. Ahammad, *J. Energy Storage*, 2020, **32**, 101908.
15 M. Bora, S. M. Benoy, J. Tamuly and B. K. Saikia, *J. Environ. Chem. Eng.*, 2021, **9**, 104986.
16 S. M. Benoy, D. Bhattacharjya, M. Bora and B. K. Saikia, *ACS Appl. Electron. Mater.*, 2022, **4**, 6322–6334.
17 Y. Zou, H. Wang, L. Xu, M. Dong, B. Shen, X. Wang and J. Yang, *J. Power Sources*, 2023, **556**, 232509.
18 K. Periyapperuma, T. T. Tran, S. Trussler, D. Ioboni and M. Obrovac, *J. Electrochem. Soc.*, 2014, **161**, A2182.
19 J. Lascovich and S. Scaglione, *Appl. Surf. Sci.*, 1994, **78**, 17–23.
20 T. R. Gengenbach, G. H. Major, M. R. Linford and C. D. Easton, *J. Vac. Sci. Technol., A*, 2021, **39**, 013204.
21 V. Dimitrov and T. Komatsu, *J. Solid State Chem.*, 2002, **163**, 100–112.
22 M. Smith, L. Scudiero, J. Espinal, J.-S. McEwen and M. Garcia-Perez, *Carbon*, 2016, **110**, 155–171.
23 G. Levi, O. Senneca, M. Causà, P. Salatino, P. Lacovig and S. Lizzit, *Carbon*, 2015, **90**, 181–196.
24 R. N. Putra, M. Halim, G. Ali, S. F. Shaikh, A. M. Al-Enizi, T. Fazal, F. J. Iftikhar and A. N. S. Saqib, *New J. Chem.*, 2020, **44**, 14035.

25 Z. Chen, H. Zhuo, Y. Hu, L. Zhong, X. Peng, S. Jing, Q. Liu, X. Zhang, C. Liu and R. Sun, *ACS Sustainable Chem. Eng.*, 2018, **6**, 7138–7150.
26 H. Teng, T.-S. Yeh and L.-Y. Hsu, *Carbon*, 1998, **36**, 1387–1395.
27 J. Wang, J. Polleux, J. Lim and B. Dunn, *J. Phys. Chem. C*, 2007, **111**, 14925–14931.
28 Y. Bai, C. Liu, T. Chen, W. Li, S. Zheng, Y. Pi, Y. Luo and H. Pang, *Angew. Chem.*, 2021, **133**, 25522–25526.
29 M. Bichat, E. Raymundo-Piñero and F. Béguin, *Carbon*, 2010, **48**, 4351–4361.
30 L. Zhang, D. Wu, Q. Ma, G. Wang, Z. Liu, M. Chang and X. Yan, *ChemElectroChem*, 2020, **7**, 838–845.
31 J. Jiang, B. Liu, G. Liu, D. Qian, C. Yang and J. Li, *Electrochim. Acta*, 2018, **274**, 121–130.
32 W.-W. Liu, X.-B. Yan, J.-W. Lang, J.-B. Pu and Q.-J. Xue, *New J. Chem.*, 2013, **37**, 2186–2195.